scientific reports

Check for updates

OPEN

Enhancing electrochromic energy storage devices with water-in-bisalt (Zn^{2+}/Al^{3+}) electrolytes for energy saving smart glass applications

Ming-Yue Tan[1], Gregory Soon How Thien[2], Kar Ban Tan[3], Ab Rahman Marlinda[4], Mohd Sufri Mastuli[5], H. C. Ananda Murthy[6], B S Surendra[7], Yun Ii Go[8] & Kah-Yoong Chan[1,2]✉

Electrochromic (EC) technology is increasingly recognized for its potential to improve energy efficiency, particularly through smart windows that modulate transparency to reduce reliance on artificial lighting and air conditioning. While EC devices generally require low external voltages to switch between colored and bleached states, further advancements are still needed to reduce energy consumption and achieve more efficient, sustainable performance. A promising solution lies in integrating EC materials with energy storage systems, offering a dual-purpose approach that enables light modulation and energy storage functionality. Numerous studies have explored zinc (Zn)-based EC energy storage devices, owing to their high theoretical specific capacity, environmental compatibility, and the abundance of zinc metal. However, the performance of Zn^{2+}-based electrolytes is often constrained by large hydrated ion sizes and a limited electrochemical stability window. To address these limitations, this study focused on investigating water-in-bisalt (WiBS) electrolytes with varying Zn^{2+}/Al^{3+} electrolyte composition to enhance both energy storage capability and EC functionality. Additionally, tungsten trioxide (WO_3) was selected as the EC material due to its proven coloration efficiency, optical modulation, and cyclic stability. Deduced from the measurement, the 10 M Zn + 3 M Al electrolyte was identified as the optimal formulation, enabling the WO_3 energy storage device to achieve an outstanding energy storage capacity of 146 mAh/m^2, excellent optical contrast (80.5%), high coloration efficiency (35.3 cm^2/C), and excellent cyclic stability of 75% after 1000 cycles. This research highlights the potential of advanced WiBS electrolytes in EC energy storage technologies, paving the way for applications in energy storage integrated smart windows and real-time energy indicators.

Electrochromic (EC) technology has recently gained attention for its energy-saving potential and environmentally friendly properties. A key application of EC devices is in smart windows, which use low voltage to regulate the amount of light and heat entering a space[1,2], thereby reducing the need for artificial lighting and air conditioning. Additionally, EC devices are energy efficient as they can sustain their colored or bleached states without requiring continuous energy input[3]. However, transitioning between these states still relies on external voltage, indicating potential for further optimization toward reduced energy consumption. Given that the mechanisms in EC devices, such as redox reaction, are similar to those in energy storage systems, there is a potential for integrating EC materials into energy storage devices[4]. Various types of energy storage systems are

[1]Faculty of Artificial Intelligence and Engineering, Multimedia University, Persiaran Multimedia, Cyberjaya 63000, Selangor, Malaysia. [2]Centre for Advanced Devices and Systems, COE for Robotics and Sensing Technologies, Multimedia University, Persiaran Multimedia, Cyberjaya 63100, Selangor, Malaysia. [3]Department of Chemistry, Faculty of Science, Universiti Putra Malaysia, Serdang 43400, Selangor, Malaysia. [4]Nanotechnology and Catalysis Research Centre (NANOCAT), Institute for Advanced Studies, Universiti Malaya, Kuala Lumpur 50603, Malaysia. [5]Faculty of Applied Sciences, Universiti Teknologi MARA, Shah Alam 40450, Selangor, Malaysia. [6]Department of Applied Chemistry, School of Applied Sciences, Papua New Guinea University of Technology, Lae 411, Morobe, Papua New Guinea. [7]Department of Chemistry, Dayananda Sagar College of Engineering, Bengaluru 560078, India. [8]School of Engineering and Physical Sciences, Heriot-Watt University Malaysia, 1, Jalan Venna P5/2, Precinct 5, Putrajaya 62200, Malaysia. ✉email: kychan@mmu.edu.my

currently being actively investigated, including batteries[5], magnetic energy storage[6], pumped hydro storage[7], and supercapacitors[8–11], each serving different energy and power demands. Among these, rechargeable battery systems, particularly zinc-based electrochemical configurations, have shown great promise for coupling energy storage with electrochromic functionality.

Zinc (Zn) metal is a popular choice for anode material in metal-based EC energy storage devices due to its high theoretical specific capacity (820 mAh/g), suitable redox potential (-0.76 V vs. Standard Hydrogen Electrode (SHE)), low toxicity, and widespread availability[12,13]. Additionally, the divalent Zn^{2+} ions released from the zinc anode play a crucial role by supplying multiple electrons during the reversible redox reaction, thereby contributing to the self-coloration feature of the device[13]. Despite their potential, the use of Zn^{2+} ion electrolytes is limited by the large size of hydrated Zn^{2+} ions, thereby impeding efficient ion intercalation[14]. Moreover, the decomposition of water molecules during Zn^{2+} deposition narrows the electrochemical stability window (ESW), thereby restricting the effective operating voltage range of the electrolyte[15]. Therefore, researchers are working on new metal salt electrolyte recipes, such as water-in-salt (WIS) and dual-ion electrolytes.

In WIS electrolytes, the high salt concentration ensures that water molecules are fully engaged in ion solvation, effectively preventing water decomposition and helping to maintain the stability of the electrolyte[14]. For instance, Wu et al. reported that the ESW of $ZnCl_2$-based WIS electrolytes increased from 1.4 V at 2 M to 2.4 V in the range of 8–10 M. The expanded ESW enabled the application of higher bleaching voltages, which in turn enhanced optical modulation, accelerated ion extraction, and improved cycling stability for over 300 cycles[14]. Similarly, Li et al.. developed a stable Zn-WO_3 flexible battery by utilizing a 30 M $ZnCl_2$ electrolyte[12]. This formulation prevented the dendrite formation, inhibited cathode dissolution, and enhanced electrochemical corrosion resistance. The resulting Zn-WO_3 battery achieved excellent capacitance retention of 94.8% after 1000 cycles. In a separate study, Tong et al. reported that the energy storage device with a 5 M calcium trifluoromethanesulfonate ($Ca(OTF)_2$) electrolyte achieved an expanded ESW of 2 V, compared to 1.38 V for the 1 M electrolyte[16]. On the other hand, the utilization of dual-ion electrolytes has been reported to improve the overall EC performance and energy storage capability of EC energy storage devices. For instance, Li et al. successfully developed rechargeable EC batteries using a hybrid Zn^{2+}/Al^{3+}-based electrolyte. The device achieved a high discharge capacity of 126.3 mAh/m^2, excellent optical contrast of 77%, and fast response times of 3.9 s for coloration and 5.1 s for bleaching[5].

Despite the proven advantages of WIS and dual-ion electrolytes, their integration as water-in-bisalt (WiBS) electrolytes, aimed at leveraging the strengths of both concepts, remains underexplored in EC energy storage devices. In particular, while the WiBS concept has been extensively studied in lithium-ion batteries[17–21], its application to EC-integrated energy storage systems has received little attention. Hence, in this study, varying concentrations of $AlCl_3$ (ranging from 0 to 7 M) were incorporated into the 10 M $ZnCl_2$ electrolyte to investigate how different compositions of the WiBS electrolytes affect the electrical and EC properties of the EC energy storage devices. Notably, a 10 M $ZnCl_2$ concentration was selected in this study, as electrolytes with concentrations of 7.4 M or higher have been reported to be classified as WIS electrolytes, characterized by a salt-to-water ratio greater than one by weight or volume[14]. Besides, Al^{3+} ions were chosen to pair with Zn^{2+} ions due to their natural abundance and trivalent nature, which contributes to a higher charge-carrier density and enables multivalent electron-transfer processes[5]. Additionally, the relatively small ionic radius of Al^{3+} (0.53 Å) could facilitate reversible intercalation into the WO_3 lattice. Such Al^{3+} insertion has been reported to enhance the structural stability and prolong the lifetime of WO_3 electrodes, attributed to its shallow insertion depth[22,23]. Furthermore, WO_3 was utilized as the EC material (cathode) in the devices to ensure that the electrolyte's performance was not constrained by the instability of the EC thin film. This choice was supported by extensive studies highlighting WO_3's exceptional coloration efficiency, optical modulation, and cyclic stability[24–27]. Unlike conventional approaches that employ either single-salt WIS electrolytes or dual-ion systems independently, this study adopts a WiBS strategy by combining high-concentration $ZnCl_2$ with $AlCl_3$, thereby integrating improved electrochemical stability with multivalent ion effects. Furthermore, systematic tuning of the bisalt composition provides deeper insight into the relationship between electrolyte design, electrochromic behavior, and energy storage performance, ultimately contributing to enhanced device stability and potential applications in energy storage window systems and energy status indicators.

Methodology

WO_3 thin film preparation

All chemicals used in this study were of analytical grade and obtained from Sigma-Aldrich, Rockville, MD, USA. Additionally, indium tin oxide (ITO) glass substrates (15 Ω/sq), serving as conductive backing, were sourced from Han Xin Industry Co., Ltd., Shanghai, China. Ingredients that were employed in the WO_3 sol-gel fabrication process included tungsten hexachloride powder (WCl_6) as the precursor, glacial acetic acid (CH_3COOH) as a chelating agent, hydrogen peroxide (H_2O_2) as an oxidizing agent, and absolute ethanol (C_2H_6O) as a solvent.

The WO_3 films in this study were prepared based on methods outlined in our previous work[25,28,29]. To initiate the process, 1 g of WCl_6 was weighed and transferred into a beaker. Subsequently, 2 mL of glacial acetic acid was added to the beaker, followed by 20 mL of ethanol. The mixture was stirred for 30 min at 200 rpm, and the color of the mixture changed from yellow to dark blue. Moving forward, 2 mL of H_2O_2 was added to the solution and stirred until a light blue color was achieved. Following that, the solution was stirred for another 2 h to attain a homogeneous clear solution. The resulting WO_3 sol-gel was kept in a glass vial and was allowed to age for 72 h. For the deposition process, the spin coating method was employed to deposit WO_3 sol-gel onto the cleaned ITO glass substrate, with a rotation speed of 3000 rpm and a duration of 30 s. Finally, the as-prepared WO_3 film was annealed in the furnace at 100 °C for 1 h.

WiBS electrolyte preparation

To prepare different compositions of Zn^{2+}/Al^{3+} electrolytes, 0.01 to 0.07 mol of $AlCl_3$ and 0.1 mol of $ZnCl_2$ were dissolved in 10 mL of distilled water. The mixture was thoroughly stirred to ensure homogeneity, resulting in solutions containing 10 M $ZnCl_2$ and 1 to 7 M $AlCl_3$.

WO_3 energy storage device construction

The EC energy storage device was constructed by assembling the structure in the following order: Glass/Zinc plate/ Zn^{2+}/Al^{3+} electrolyte/WO_3 thin film/ITO, as illustrated in Fig. 1. To further elaborate, the anode (zinc plate) and cathode (WO_3 thin film) were assembled in a parallel configuration, with metal salt electrolyte sandwiched between them. Finally, the device was sealed using UV resin to prevent electrolyte leakage. Notably, the EC energy storage devices exhibited an active area of 2.4 cm^2.

Characterization techniques

The thickness and structural properties of the WO_3 thin films were characterized using field emission scanning electron microscopy (FESEM, Nova NanoSEM 450) and X-ray diffractometer (XRD, Shimadzu) with Cu Kα radiation (λ = 1.5406 Å) over the 2θ range of 20 to 70°. Besides, the elemental composition of the colored WO_3 thin films was analyzed using X-ray photoelectron spectroscopy (XPS, JEOL JPS-9200). Prior to peak fitting, the XPS spectra were baseline-corrected using a Shirley background. The individual peaks were subsequently deconvoluted using Gaussian-Lorentzian functions, and the fitting parameters (peak position, width, and intensity) were iteratively refined until a good agreement between the experimental and fitted curves was achieved. Furthermore, the viscosity of the electrolyte was measured using a viscometer (Anton Paar SVM 3000). Moreover, the electrical properties of the EC energy storage devices were measured using electrochemical impedance spectroscopy (EIS, Gamry Interface 1010E Potentiostat) and galvanostatic charge/discharge (GCD, Gamry Interface 1010E Potentiostat) techniques. Furthermore, the optical transmittances of the devices were examined using an ultraviolet-visible (UV-Vis, Avantes spectrophotometer AvaSpec-2048 L) spectrophotometer. Lastly, EC performance was investigated using chronoamperometry (CA) and cyclic voltammetry (CV) measurements (Autolab PGSTAT204). A two-electrode electrochemical configuration was employed, where the WO_3 thin film functioned as the working electrode and ITO served as the counter electrode. Notably, all testing was performed under ambient air conditions at room temperature.

Results and discussion

Working mechanism of WO_3 energy storage device

Prior to investigating the fundamental characteristics and performance of the WO_3 energy storage device, it is essential to first understand its working principle. Figure 2 depicts the cross-section of a WO_3 energy storage device and demonstrates how redox electrochemical reactions take place in it.

During the discharging/coloring process, the Zn anode underwent oxidation by releasing electrons ($Zn \rightarrow Zn^{2+} + 2e^-$), thereby generating electric power through the external circuit[30]. Simultaneously, the Zn^{2+} and Al^{3+} ions migrated through the electrolyte and intercalated into the WO_3 thin film, reducing W atoms from W^{6+} to W^{5+}, which caused the thin film to turn blue. Interestingly, the co-insertion of multiple ions into a single electrode was feasible if their intercalation voltage ranges overlapped within the operating window[31]. Conversely, during the charging/bleaching process, Zn^{2+} and Al^{3+} ions were extracted from the WO_3 thin film, with Zn^{2+} subsequently plated onto the Zn plate. Consequently, the WO_3 thin film reverted to its transparent state. The redox process can be expressed by Eqs. (1)-(2)[14,22]:

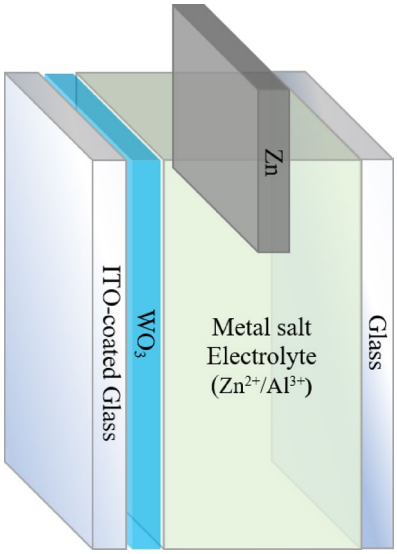

Fig. 1. Electrochromic energy storage device structure.

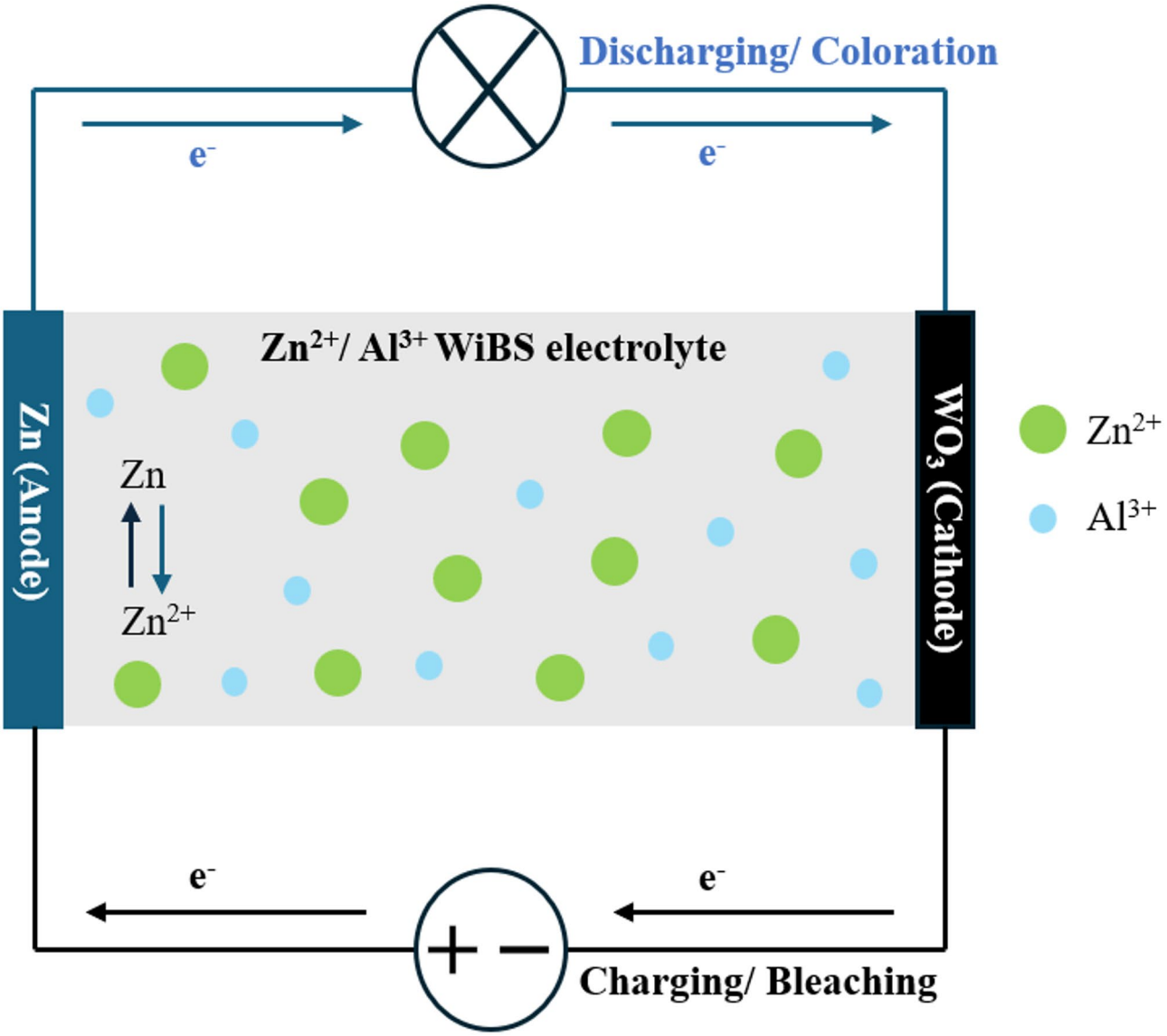

Fig. 2. Redox electrochemical reactions in the WO_3 energy storage device.

$$WO_3 + xZn^{2+} + 2xe^- \leftrightarrow Zn_xWO_3 \quad (1)$$

$$WO_3 + yAl^{3+} + 3ye^- \leftrightarrow Al_yWO_3 \quad (2)$$

Structural properties of WO_3 thin film

The XRD patterns of the WO_3 thin film, as shown in Fig. 3**(a)**, reveal a broad peak at approximately 25°, confirming its amorphous nature (ICDD No.: 01-087-2380)[32]. The amorphous structure was attributed to the low post-annealing temperature of 100 °C. Additionally, the FESEM image in Fig. 3**(b)** further demonstrates a film thickness of 286 nm. In this study, a temperature of 100 °C and a thickness close to 300 nm were selected, as our earlier work[25,33] demonstrated that amorphous WO_3 thin films prepared under these conditions exhibited high optical modulation and excellent color efficiency. Moreover, a thickness of around 300 nm provided optimal color appearance while maintaining efficient ion transport, avoiding the limitations associated with excessively thick films. These features made such WO_3 films highly desirable as cathode materials in EC energy storage devices.

Elemental compositions of colored WO_3 thin film

The colored WO_3 thin film was analyzed using XPS to examine its elemental composition and the valence states of the elements involved. The XPS spectrum in Fig. 4 confirm the presence of four key elements: Al, Zn, W, and O within the intercalated WO_3 film.

Figure 4**(a)** displays a peak at 1022.7 eV, corresponding to the binding energy of the Zn $2p_{3/2}$ orbital, along with a second peak at 1045.8 eV, representing the Zn $2p_{1/2}$ orbital. These two peaks, separated by approximately

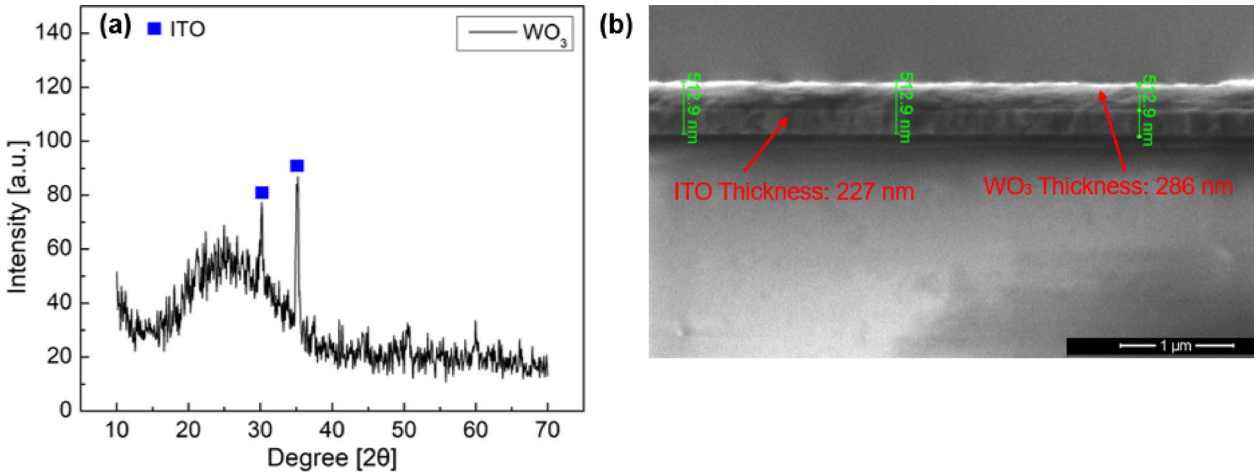

Fig. 3. (**a**) XRD and (**b**) Cross-section measurement of WO_3 thin film.

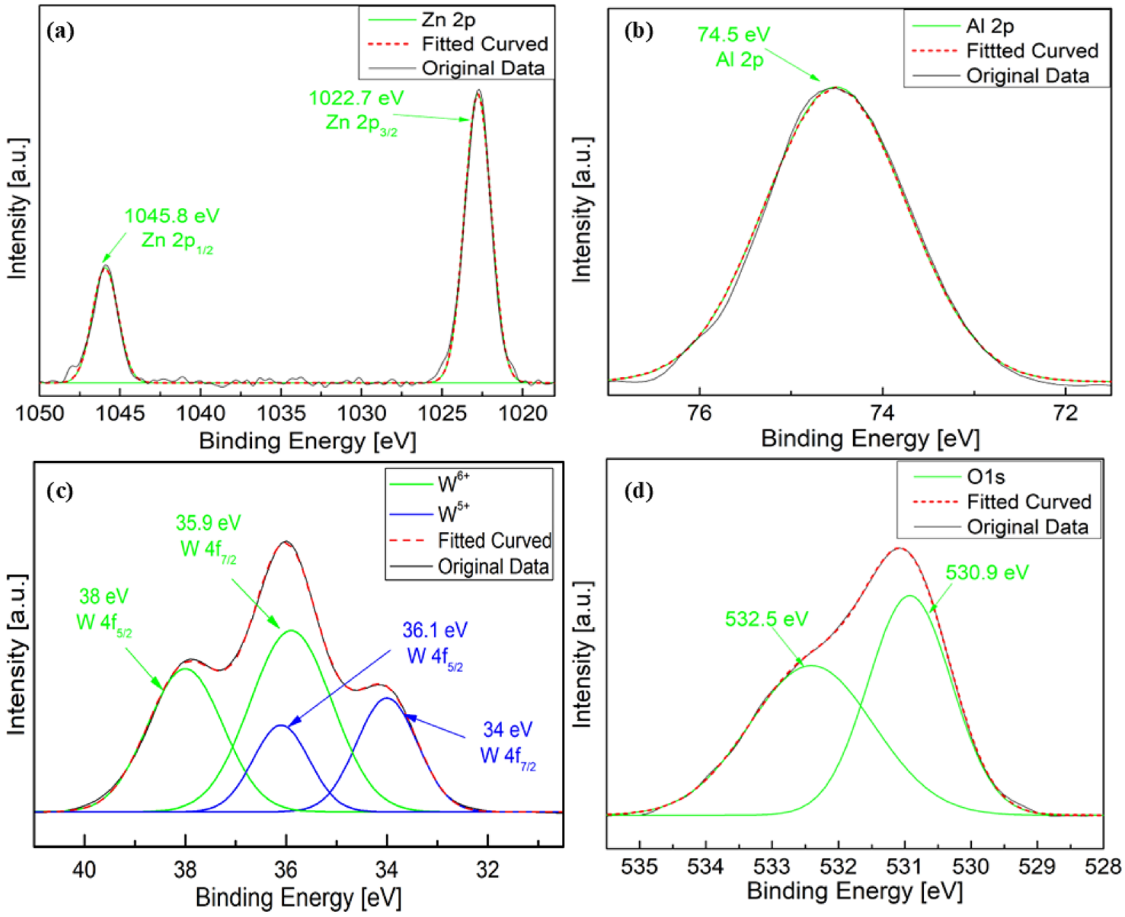

Fig. 4. XPS spectrum of (**a**) Zn 2p (**b**) Al 2p, (**c**) W 4f, and (**d**) O 1s in colored WO_3 thin film.

23 eV, reflected the expected spin-orbit splitting of the Zn 2p orbital and were consistent with the binding energy values for Zn^{2+}[34]. Furthermore, Fig. 4**(b)** reveals a binding energy of 74.5 eV, which corresponds to the Al 2p orbital, confirming the presence of Al in its + 3 oxidation state (Al^{3+})[35]. These findings indicated that both Al^{3+} and Zn^{2+} ions participated in the coloring process during the discharging cycle.

In addition, Fig. 4**(c)** displays peaks at 36.1 eV and 38 eV corresponding to the W $4f_{5/2}$ orbital, while peaks at 35.9 eV and 34 eV correspond to the W $4f_{7/2}$ spin-orbit, consistent with previously reported literature[36,37]. The stronger peaks at 38 eV and 35.9 eV were attributed to W^{6+} species, whereas the weaker peaks at 36.1 eV

and 34 eV represented W^{5+}. The presence of W^{5+} species indicated the existence of oxygen vacancies and the insertion of Zn^{2+} and Al^{3+} ions into the WO_3 film, which induced the observed color change. Furthermore, the O 1s spectrum of the thin film (Fig. 4**(d)**) was deconvoluted into two components centered at 530.9 eV and 532.5 eV. The dominant peak at 530.9 eV corresponded to lattice oxygen bonded to tungsten atoms in the WO_3 framework, while the higher binding energy peak at 532.5 eV was attributed to oxygen vacancies or adsorbed water[38,39].

Electrical properties of WO_3 energy storage devices

Figure 5**(a)** presents the Nyquist plot of WO_3 energy storage devices using a 10 M Zn electrolyte with varying Al concentrations (1-7 M), measured through EIS. Notably, the diameter of the semicircle in the plot represented the charge-transfer resistance (R_{ct}) of the devices. The findings revealed that the device with 10 M Zn electrolyte exhibited the largest impedance curve, signifying the highest resistivity of 1970 Ω. Interestingly, the addition of 2 M and 3 M Al salt to the 10 M $ZnCl_2$ solution significantly reduced the R_{ct} to 90 Ω and 55 Ω, respectively. However, further additions of 7 M Al salt resulted in increased resistances of 715 Ω. To elucidate these observations, the conductivity (σ) of the electrolytes was determined from the R_{ct} values using Eq. (3):

$$\sigma = \frac{L}{R_{ct} \cdot A} \tag{3}$$

where L is the distance between electrodes (0.25 cm) and A is the surface area of the WO_3 electrode (2.4 cm^2). Additionally, the viscosity of the electrolytes was measured using a viscometer to assess how variations in electrolyte concentration influenced their resistivity and conductivity [see Fig. 5**(b)**].

Figure 5 **(b)** reveals that introducing Al salt concentrations from 1 M to 3 M enhances ionic conductivity by increasing the availability of charge carriers and improving charge transfer at the interface between the electrolyte and the WO_3 film. Concurrently, the electrolyte viscosity increases from 6.3 mPa·s at lower concentrations to 15.3 mPa·s at 3 M. However, when the Al concentration exceeded 3 M, the viscosity rose sharply to 61.2 mPa·s, which impeded ion mobility within the WO_3 film[14]. Consequently, there was an increase in resistivity and a corresponding decline in conductivity. Notably, the optimal Al concentration for achieving the highest conductivity (1.94 mS/cm) was found to be 3 M, where a favorable balance was achieved between ion availability, ion mobility, and electrolyte viscosity. Moreover, the results indicated that the WiBS electrolyte with 3 M Al salt exhibited a conductivity 35 times greater than that of the standalone WIS Zn^{2+} electrolyte. This observation demonstrated that introducing an appropriate concentration of Al salt into the WIS Zn^{2+} electrolyte could significantly improve its ionic conductivity.

The energy storage capacities of the devices with various compositions of WiBS electrolytes are assessed through the galvanostatic charge/discharge (GCD) technique at a current density of 0.5 mA/cm^2, as depicted in Fig. 6**(a)**. The results demonstrated that the device with 10 M Zn electrolyte had the lowest discharge capacity, yielding 17 mAh/m^2. When 1 M of Al was introduced, the discharge capacity increased to 35 mAh/m^2, demonstrating an initial improvement. The discharge capacity peaked at 146 mAh/m^2 with the addition of 3 M Al, suggesting that this electrolyte composition optimally enhanced the device's energy storage capability. This improvement was attributed to the co-insertion of Zn^{2+} and Al^{3+} ions, which increased the number of active charge carriers and facilitated better ionic transport within the electrolyte[31,40]. However, as the Al concentration was further increased to 7 M, the discharge capacity dropped to 77 mAh/m^2. This observation aligned with the ionic conductivity results, where the increased viscosity of the electrolyte at higher concentrations impeded ion mobility and hindered the energy storage process.

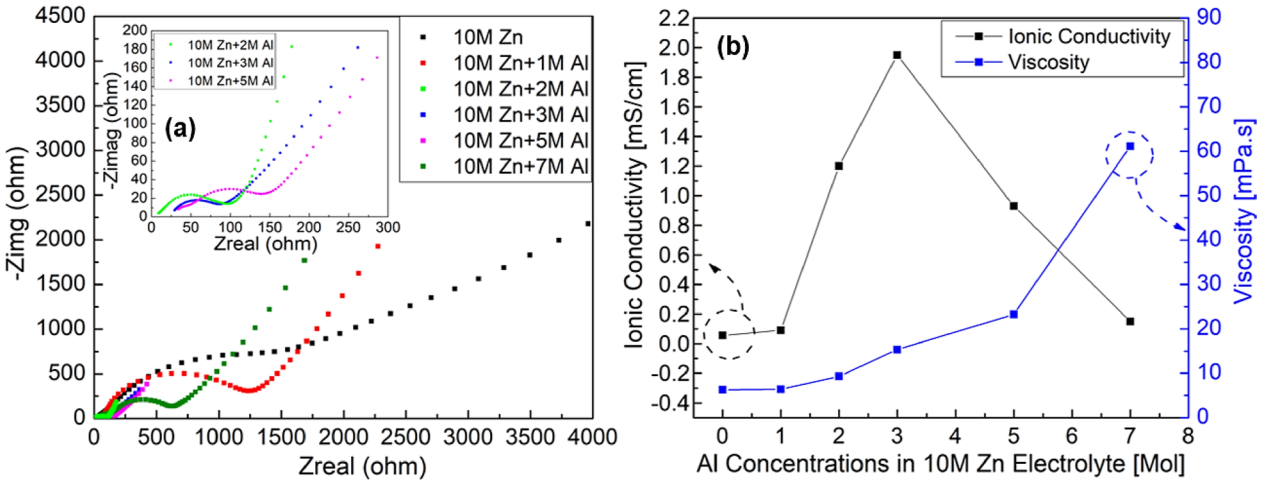

Fig. 5. (**a**) EIS measurements and (**b**) conductivity and viscosity data of WO_3 energy storage devices with 10 M Zn electrolyte and varying Al concentrations.

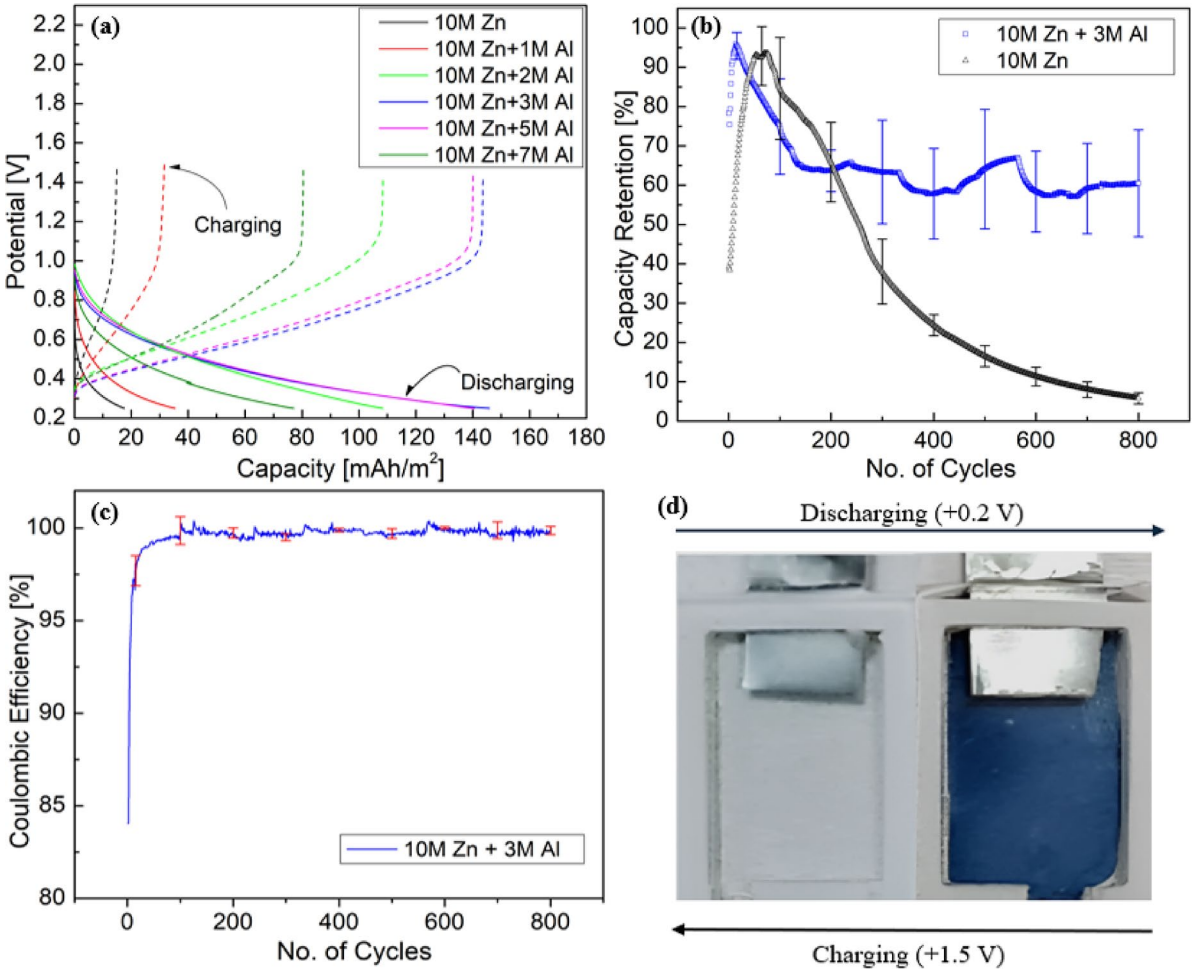

Fig. 6. (**a**) GCD curves of WO_3 energy storage devices with 10 M Zn electrolyte and varying Al concentrations (**b**) capacity retention of WO_3 energy storage devices with 10 M Zn and 10 M Zn + 3 M Al electrolytes over 800 cycles (**c**) coulombic efficiency of WO_3 energy storage devices with 10 M Zn + 3 M Al electrolytes over 800 cycles (**d**) color changes in WO_3 energy storage devices (10 M Zn + 3 M Al) during charging and discharging cycle.

Moreover, GCD cycling was conducted to evaluate the long-term electrochemical stability of the devices, where capacity fading could arise from interfacial side reactions, and structural degradation of the cathode material, such as microcrack formation or partial structural collapse, which hinder reversible ion transport[41]. Since the electrolyte containing 10 M Zn + 3 M Al demonstrated the highest energy storage capacity, it was compared with the standalone 10 M Zn electrolyte to assess their capacity retention over 800 cycles. The results were averaged from three devices, and the error bars represented the corresponding device-to-device variation. Figure 6(**b**) reveals that the device using the 10 M Zn + 3 M Al electrolyte experiences an initial capacity decline, but the capacity stabilizes at approximately 60% after extended cycling, reflecting excellent electrochemical stability. In contrast, the device using the 10 M Zn electrolyte exhibited a rapid and continuous decrease in capacity with increasing cycle number, suggesting severe performance degradation over long-term operation. Moreover, as shown in Fig. 6(**c**), the coulombic efficiency of the device with the 10 M Zn + 3 M Al electrolyte remains stable throughout cycling and achieves an average value of approximately 99% after 800 cycles. These results indicated that the incorporation of Al^{3+} additives significantly enhanced capacity retention by suppressing the formation of harmful by-products, such as Zn-based salts on the WO_3 thin film, while simultaneously inhibiting zinc dendrite growth on the Zn plate. In addition, the inserted Al^{3+} ions formed strong chemical interactions with oxide ions in the WO_3 lattice, thereby reinforcing lattice stability and mitigating thin-film dissolution or structural collapse during prolonged cycling[42].

Furthermore, color changes were observed during the charging-discharging cycles, enabling the EC energy storage device to serve as an energy status indicator. This feature provides a simple and intuitive way for users to monitor the device's energy level by observing the color contrast. As illustrated in Fig. 6(**d**), the device transitions to a blue color during discharge (+0.2 V) and reverts to a transparent state upon charging (+1.5 V), driven by the redox reactions within the device.

Figure 7 illustrates the open circuit voltage (OCP) of the EC energy storage devices, measured using a multimeter. Notably, the OCP was obtained 10 min after a full charge to ensure electrochemical equilibrium

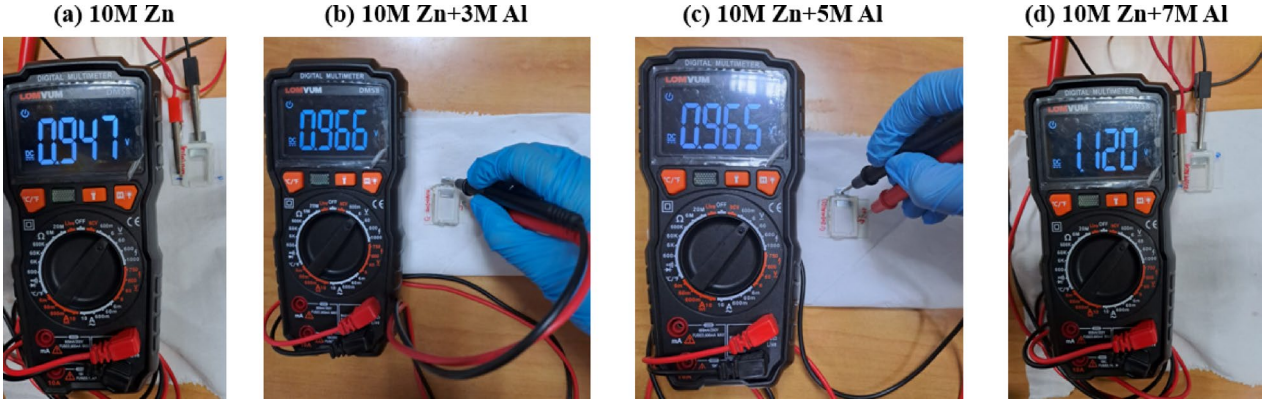

Fig. 7. Open circuit potential of WO_3 energy storage devices with 10 M Zn electrolyte and (**a**) 0 M Al (**b**) 3 M Al (**c**) 5 M Al (**d**) 7 M Al.

was reached within the device, where no further redox reactions were occurring between the electrodes[43]. Generally, the OCP is primarily determined by the difference between the standard electrode potentials of the active electrode materials. Given that the potential of the Zn electrode is − 0.76 V (vs. SHE) and that of WO_3 is + 0.3 V (vs. SHE), the theoretical OCP was calculated to be 1.06 V[12,44].

The results of this study showed that the OCP of the devices ranged between 0.94 and 1.1 V, which closely aligned with the theoretical predictions. The slight deviations from the theoretical values and discrepancies with other studies were attributed to factors such as the choice and concentration of the electrolyte, variations in the electrode material, as well as the overall configuration of the device[45–47]. Notably, the highest OCP of 1.1 V was observed with the addition of 7 M Al, suggesting that a higher electrolyte concentration influenced the chemical potentials at the electrode surfaces, thereby increasing the voltage output[48,49].

The OCP, along with the inherent charge storage capabilities of these devices, enabled them to perform dual functions: self-coloring and supplying energy to low-voltage electrical appliances. To showcase these functionalities, four EC energy storage devices were connected in series, generating a combined voltage exceeding 3 V, which was sufficient to power a small LED [see Fig. 7]. Remarkably, the devices not only illuminated the LED but also simultaneously transitioned from a transparent state to a dark blue color, thereby demonstrating their self-coloring capability. Importantly, no external voltage was applied throughout this process, highlighting the potential of these devices for future energy-saving window systems.

Electrochromic (EC) properties of WO_3 energy storage devices

Linear sweep voltammetry was performed at a scan rate of 0.1 V/s to investigate the electrochemical stability window (ESW) of WiBS electrolytes. Notably, the ESW was identified as the potential range where the current remains near zero, indicating a stable region without water decomposition[50]. Figure 9 shows that the ESW for all electrolytes ranges from 2.0 to 2.4 V, demonstrating excellent electrochemical stability. This result was attributed to the high concentration of salt in the electrolytes (WIS structure), which effectively suppressed the electrolysis of water molecules (H_2O)[14]. A related study by Wu et al.[14] demonstrated that the 8 to 20 M $ZnCl_2$ electrolyte achieved a higher ESW of 2.4 V, compared to 1.4 V for a 2 M $ZnCl_2$ electrolyte, which further validates these findings. Similarly, Zhang et al.[51] observed that increasing the concentration of $ZnCl_2$ solutions from 5 M to 30 M expanded the electrochemical window from 1.6 to 2.3 V. The authors further explained that the expansion was attributed to the improved zinc deposition efficiency and reduced hydrogen evolution.

The cyclic voltammetry (CV) curves of the WO_3 energy storage devices with various WiBS electrolyte compositions are illustrated in Fig. 8**(a)**. These CV measurements were carried out over a voltage range from 0.2 to 1.5 V at a scan rate of 0.1 V/s, using a potentiostat analyzer. Figure 8**(a)** demonstrates a clear trend wherein the cathodic peak current of the devices incorporating WiBS electrolytes is significantly higher than that of the standalone 10 M WIS Zn electrolyte. Specifically, the 10 M Zn electrolyte exhibited a relatively low cathodic peak current of -0.87 mA. Upon the addition of 1 M Al salt, the cathodic peak current increased to -1.23 mA, indicating a substantial enhancement. This trend continued as the Al salt concentration increased to 3 M, reaching a maximum cathodic peak current of -3.02 mA. These observations were attributed to the addition of appropriate amounts of Al salt to the 10 M Zn solution, which introduced smaller and highly mobile Al^{3+} ions that could efficiently participate in the redox reactions[14]. Besides, the amorphous WO_3 thin film played a crucial role, as its porous and high surface area facilitated easier ion diffusion during the redox reaction[25].

Furthermore, WO_3 energy storage devices utilizing 10 M Zn, 10 M Zn + 3 M Al, and 10 M Zn + 7 M Al electrolytes were evaluated at varying scan rates from 25 to 150 mV/s to investigate their electrochemical kinetics, as shown in Fig. 10**(b–d)**. The results revealed that higher scan rates led to increased anodic ($I_{p.a.}$) and cathodic (I_{pc}) peak currents, attributed to the greater current passing through the film. Additionally, a linear relationship between $I_{p.a.}$ and I_{pc} versus the square root of the scan rate (25–150 mV/s) was observed, indicating that the electrochemical process in the devices was diffusion-controlled[23].

Optical modulation is a crucial parameter in assessing the EC performance of WO_3 energy storage devices. Typically, achieving excellent optical contrast requires a high transmittance in the bleached state and a low

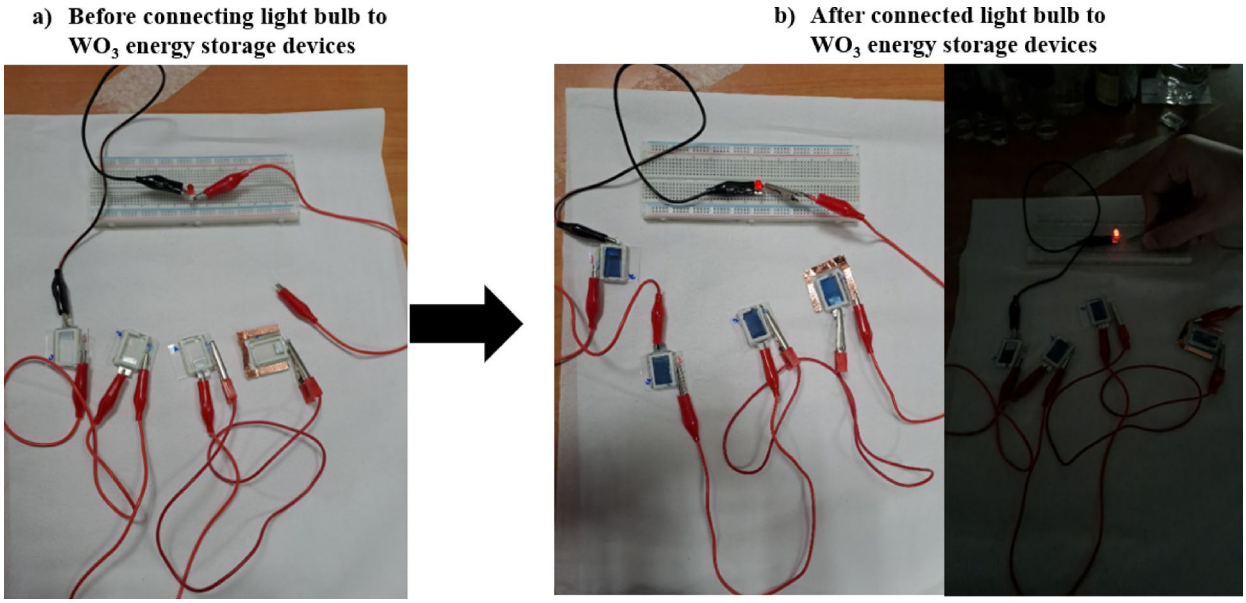

Fig. 8. (**a**) Before and (**b**) after connecting the light bulb to WO_3 energy storage devices.

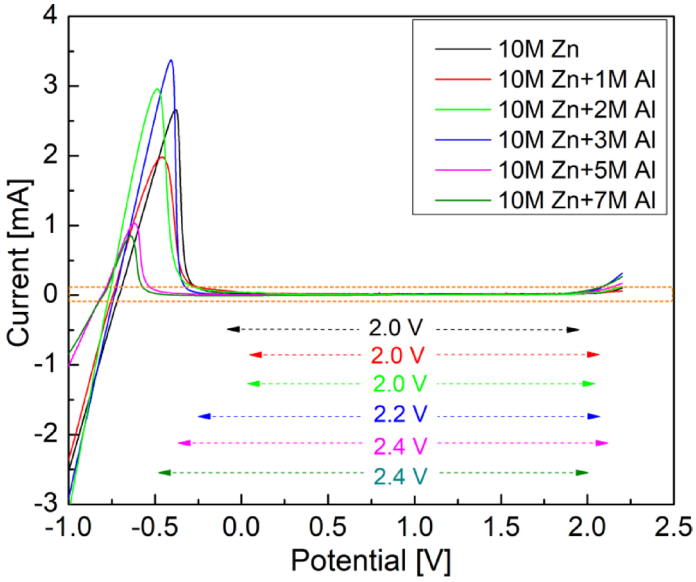

Fig. 9. Linear sweep voltammetry of WO_3 energy storage devices with 10 M Zn electrolyte and varying Al concentrations.

transmittance in the colored state. To evaluate this contrast, chronoamperometry (CA) measurements were performed on the WO_3 energy storage devices using step potentials of +0.2 V and +1.5 V. Simultaneously, optical transmittance at a wavelength of 633 nm was measured using UV-vis spectroscopy. Figure 10 illustrates the optical contrast of devices using different WiBS electrolyte compositions, while Table 1 tabulates the coloring, bleaching, and optical transmittance values corresponding to each electrolyte composition.

As shown in Fig. 11, devices utilizing 10 M Zn + 2 M Al and 10 M Zn + 3 M Al electrolyte combinations exhibit high optical modulation of 73.4% and 80.5%, respectively. The high optical contrast was attributed to their low coloring transmittance (13.3% for 10 M Zn + 2 M Al and 10.7% for 10 M Zn + 3 M Al) paired with high bleaching transmittance (86.7% and 91.2%, respectively), making them well-suited for applications requiring prominent visual transitions, such as smart windows and display technologies. Conversely, devices with other compositions, such as 10 M Zn + 1 M Al and 10 M Zn + 7 M Al, displayed lower optical modulation values of 44.2% and 46.9%, respectively, indicating less contrast between colored and bleached states. The low optical contrast was likely attributed to their poor ionic conductivity, as indicated by the EIS measurements.

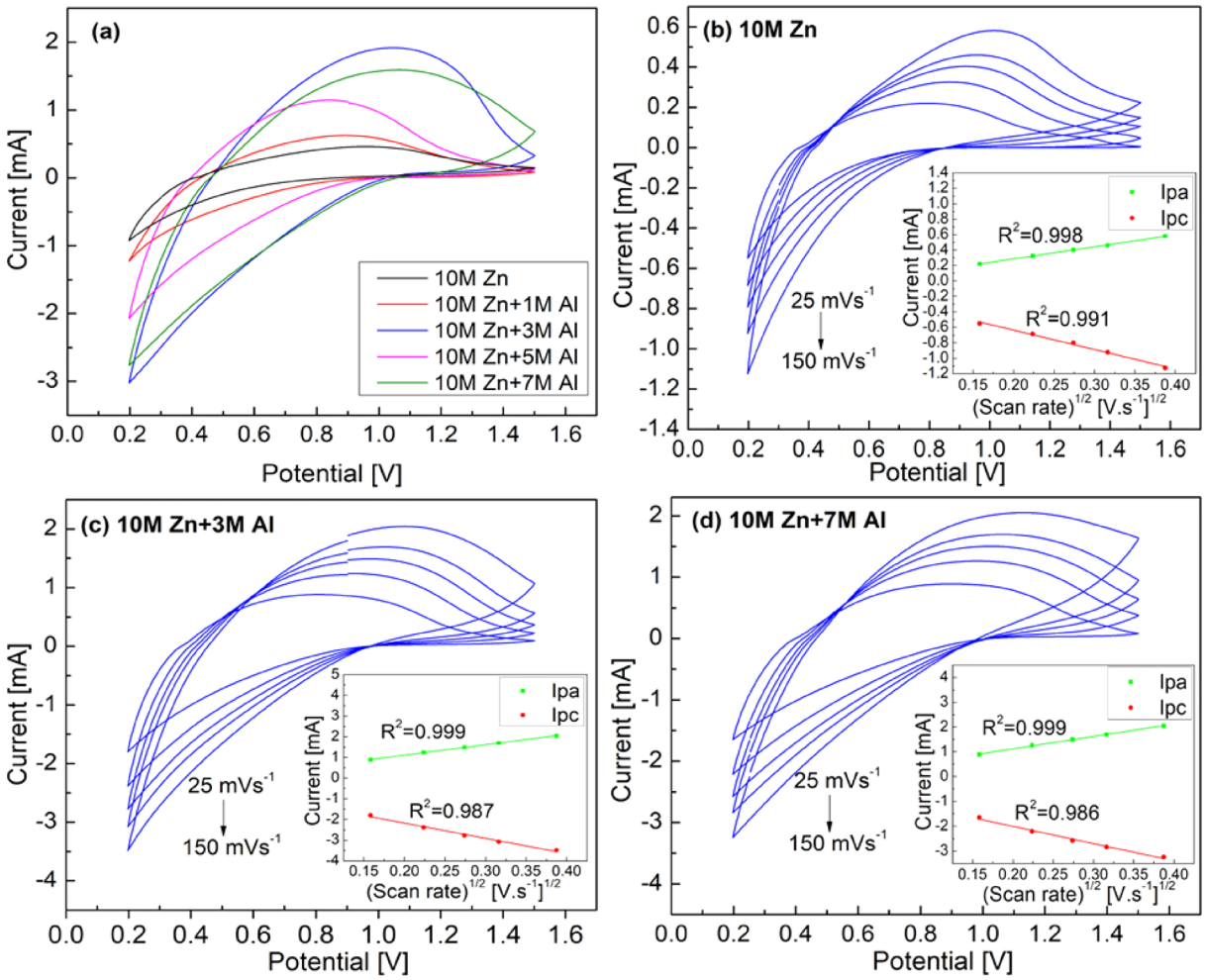

Fig. 10. Cyclic voltammograms of WO_3 energy storage devices: (**a**) Comparison of CV profiles for devices with varying WiBS compositions at a scan rate of 0.1 V/s; (**b**–**d**) CV curves for devices using 10 M Zn, 10 M Zn + 3 M Al, and 10 M Zn + 7 M Al electrolytes at scan rates of 25–150 mV/s.

Electrolytes	Coloring Transmittance, T_c (%)	Bleaching Transmittance, T_b (%)	Optical Modulation, ΔT (%)
10 M Zn	40.32	86.22	45.90
10 M Zn + 1 M Al	52.64	96.85	44.20
10 M Zn + 2 M Al	13.27	86.70	73.43
10 M Zn + 3 M Al	10.74	91.24	80.49
10 M Zn + 5 M Al	16.0	85.57	69.57
10 M Zn + 7 M Al	34.81	81.69	46.87

Table 1. Coloring and bleaching transmittance of WO_3 energy storage devices with 10 M Zn electrolyte and varying Al concentrations.

Furthermore, three WO_3 energy storage devices using the 10 M Zn + 3 M Al electrolyte composition underwent cyclic stability testing over 1000 cycles (80000 s), evaluated through continuous CA measurements while monitoring optical transmittance and modulation [see Fig. 12(**a**) and (**b**)]. The results showcased outstanding cyclic stability, with degradation in average optical modulation from 85% to 75% and an average charge balance of 95% [see **Fig. S1**] over the test period, indicating reliable performance during prolonged operation. Optical degradation in EC devices was commonly associated with incomplete ion extraction and accumulated lattice distortion during repeated coloration-bleaching processes, leading to a reduced change in optical transmittance. In this system, the presence of Al^{3+} ions helped mitigate these effects by stabilizing the WO_3 framework. As reported by Guo et al., the improved EC stability associated with Al^{3+} ions was attributed to their smaller ionic radius, which minimized lattice expansion[23]. The authors further suggested that the strong

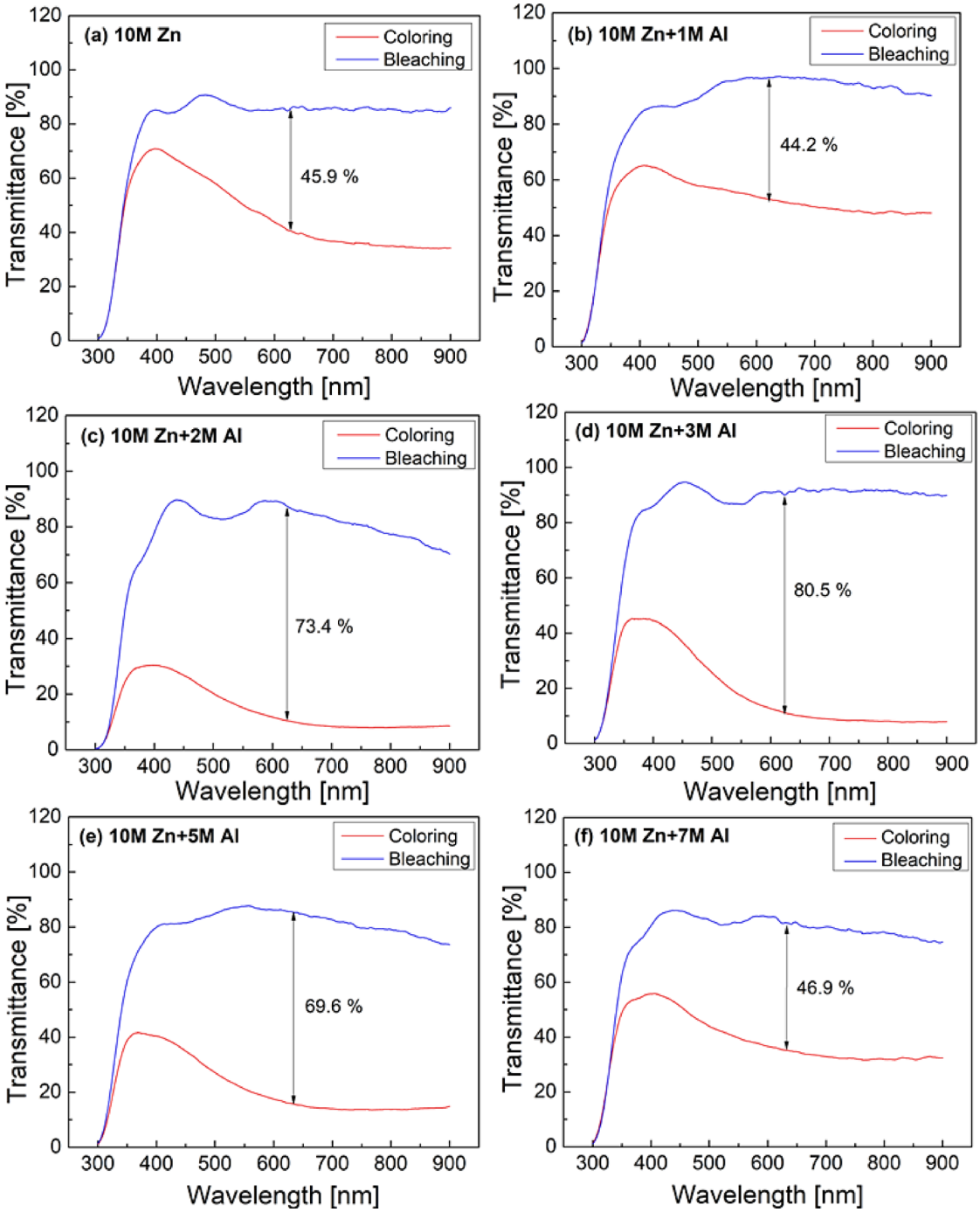

Fig. 11. Coloring and bleaching transmittance of WO_3 energy storage devices with 10 M Zn electrolyte and (**a**) 0 M Al, (**b**) 1 M Al, (**c**) 2 M Al, (**d**) 3 M Al, (**e**) 5 M Al, (**f**) 7 M Al.

electrostatic forces resulting from the Coulombic interactions between Al^{3+} ions and the amorphous WO_3 film contributed to stabilizing the crystal structure, thereby enhancing the device's lifespan[23].

Table 2 summarizes the coloring and bleaching kinetics of WO_3 energy storage devices with a 10 M Zn electrolyte and varying Al concentration. The key parameters included coloring time (t_c), bleaching time (t_b), optical density (ΔOD), intercalated charges (Q_{in}), and coloration efficiency (CE).

The findings revealed that the device with 10 M Zn electrolyte had a coloring time of 48 s, rendering it the slowest in achieving the colored state. However, when Al salt was introduced, the coloring time decreased significantly, as seen in the 10 M Zn + 3 M Al composition, which achieved one of the fastest coloring times at 18.2 s. This observation was attributed to the improved ionic conductivity of the electrolyte and the presence of the small, lightweight Al^{3+} ion, which accelerated ion transport to the WO_3 layer and facilitated faster coloration[5]. Furthermore, this composition exhibited the highest optical density of 0.93, indicating its ability to absorb light

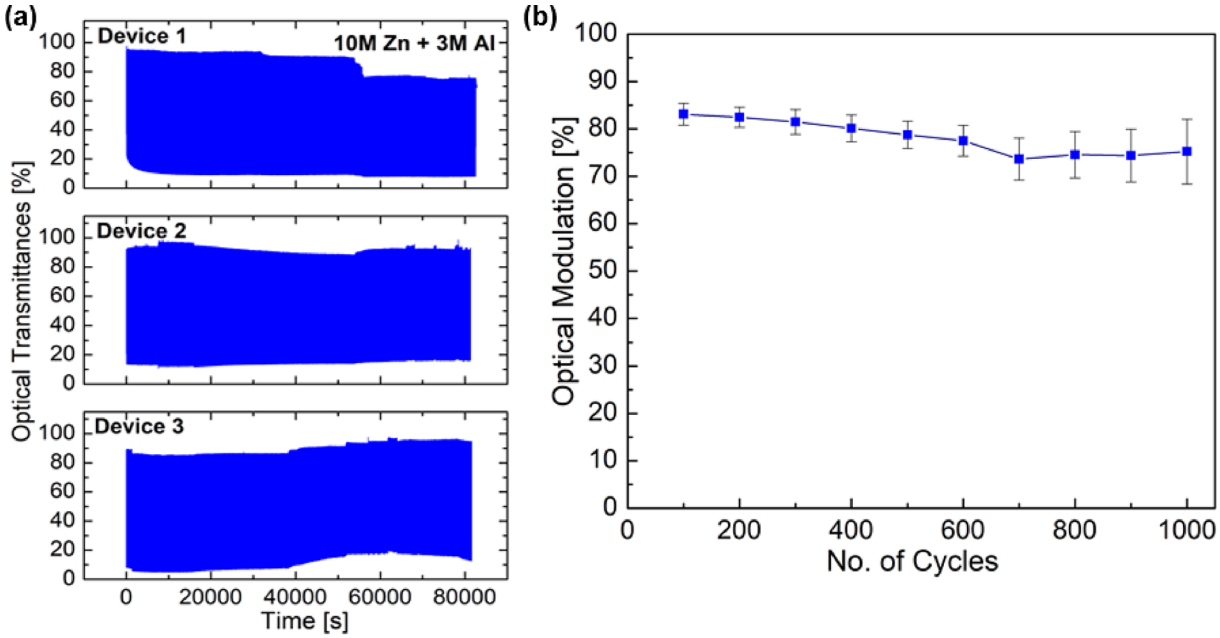

Fig. 12. (**a**) Optical transmittance of three identical WO_3 energy storage devices (Device 1–3) with 10 M Zn + 3 M Al electrolyte (**b**) Average optical contrast of WO_3 energy storage devices (10 M Zn + 3 M Al) over 1000 cycles.

Electrolytes	Coloring Time, t_c (s)	Bleaching Time, t_b (s)	Optical Density, ΔOD	Intercalated Charges, Q_{in} (C/cm^2)	Coloration Efficiency, CE (cm^2/C)
10 M Zn	48	3.22	0.33	-0.007	44.00
10 M Zn + 1 M Al	39	4.12	0.26	-0.009	29.31
10 M Zn + 2 M Al	27.3	5.40	0.82	-0.022	37.30
10 M Zn + 3 M Al	18.2	5.03	0.93	-0.026	35.32
10 M Zn + 5 M Al	22.8	3.82	0.73	-0.021	34.20
10 M Zn + 7 M Al	13.5	7.62	0.37	-0.021	17.39

Table 2. Coloring and bleaching kinetics of WO_3 energy storage devices with 10 M Zn electrolyte and varying Al concentrations.

and produce a strong color contrast. Additionally, the coloring time for all WO_3 energy storage devices was longer than the bleaching time, as the device experienced greater resistance during the transition from the insulating WO_3 state to the conductive tungsten bronze phase (Zn_xWO_3 and Al_xWO_3). In contrast, the ion extraction process during bleaching benefited from the higher electronic conductivity of the colored state, allowing it to proceed more rapidly[52]. The observation was consistent with the previous findings[33,52,53]. Remarkably, Table 2 shows that all devices demonstrate a rapid bleaching time of less than 10 s, primarily due to the wide ESW of the WIS and WiBS electrolytes, which supports the application of higher bleaching voltages. Consequently, Zn^{2+}/Al^{3+} ions were efficiently extracted from the WO_3 films during the bleaching cycle, minimizing the risk of cation trapping within the EC layer[14].

Coloration efficiency (CE) is defined as the ratio of optical density (ΔOD) to the intercalated charge per unit area, as expressed in Eq. (4)[54]:

$$CE = \frac{\Delta\ (OD)}{Q_{in}} = \frac{log\left(\frac{T_b}{T_c}\right)}{Q_{in}} \tag{4}$$

where T_b is the bleaching transmittance, T_c is the coloring transmittance, and Q_{in} is the intercalated charge per unit area. Table 3 highlights that the device containing 10 M Zn electrolyte achieves the highest CE value of 44 cm^2/C. However, a decrease in CE was observed when Al salt was added to the electrolyte. These findings indicated a trade-off: while incorporating Al salt could enhance optical contrast and speed up switching time, it also compromised the CE. This trade-off arose because a larger amount of charge was intercalated into the thin film to achieve a deeper colored state. As more charge was consumed to generate sufficient optical absorption, the resulting optical density change (ΔOD) per unit charge decreased, leading to a lower CE and potentially

Authors	Electrolytes	Electrode	Film/ Device	Applied Voltage (V)	Energy storage capacity (mAh/m^2)	Switching time (s)	Optical Modulation (%)	Coloration Efficiency (cm^2/C)	Cycles
Li et al.[5]	1 M $ZnSO_4$-$AlCl_3$	WO_3	Device	0.1/1.2	126.3	t_c: 5.7 t_b: 10.3	77% @ 632.8 nm	-	200
Wu et al.[14]	20 M $ZnCl_2$	WO_3	Device	0/2	-	t_c: 4.8 t_b: 3.6	64% @ 660 nm	-	300
Eric et al.[22]	DMSO-modified hydrogel (1 M $ZnSO_4$ + 1 M $AlCl_3$)	WO_3	Device	0.4/1.2	175	-	80% @ 632 nm	54	1000
Cai et al.[55]	0.5M H_2SO_4	CeO_2/TiO_2 with WO_3/ PED-OT: PSS	Device	-0.7/1	25	t_c: 12.7 t_b: 15.8	73.2% @ 633 nm	108.9	200
This work	10 M $ZnCl_2$ + 3 M $AlCl_3$	WO_3	Device	0.2/1.5	146	t_c: 18.2 t_b: 5.03	80.5% @ 633 nm	35.3	1000

Table 3. A comparison table of electrical and EC parameters of WO_3 energy storage devices between the current study and others.

higher energy consumption in practical applications. Fortunately, the device incorporating 2 M and 3 M Al salt maintained a relatively high CE of 37.3 cm^2/C and 35.32 cm^2/C, respectively, which was attributed to their high optical density.

Moreover, Table 3 summarizes the experimental results from this study, enabling a comparison of the electrical and EC parameters of the WO_3 energy storage devices with those reported in other studies. In comparison to previous studies, this work utilized the unique properties of WiBS electrolytes to improve the EC and energy storage performance of WO_3 energy storage devices. The energy storage capacity achieved in this study (146 mAh/m^2) surpassed that reported by Li et al.[5](126.3 mAh/m^2, using a 1 M $ZnSO_4$-$AlCl_3$ electrolyte), attributed to the enhanced ion conductivity and stability provided by the WiBS configuration. Besides, the optical modulation demonstrated in this study (80.5%) was comparable to that of Eric et al.[22](80%, using a DMSO-modified hydrogel electrolyte) and exceeded the values reported for systems utilizing standalone WIS or dual-ion electrolytes. Nevertheless, the CE of this work (35.3 cm^2/C) remained lower than those reported by Cai et al.[55](108.9 cm^2/C) and Eric et al.[22](54 cm^2/C). Despite this limitation, the device exhibited outstanding cyclic stability, maintaining consistent performance over 1000 cycles, underscoring its balance of optical modulation, energy storage capacity, and durability. These findings established the proposed system as a competitive and promising candidate for advanced EC energy storage applications.

Challenges in practical device implementation

For the practical implementation of the EC energy storage device in applications such as smart windows, challenges related to scalability, manufacturability, and cost must be addressed. Achieving uniform and high-quality EC thin films over large-area substrates requires industry-compatible deposition techniques, including DC or RF magnetron sputtering, roll-to-roll processing, and spray coating, which allow precise control of nanoscale film thickness (~ 300 nm) to maintain consistent optical modulation across the device. In addition, the reliance on high-purity transition metal oxides, vacuum-based sputtering infrastructure, and indium-based transparent conductive electrodes contributes significantly to manufacturing costs, motivating the exploration of cost-effective alternatives such as hybrid transparent electrodes that combine ITO with metal mesh structures and the use of multivalent-ion-based electrolytes as substitutes for conventional lithium-based systems[56]. For practical deployment, solid-state or gel-based electrolytes that effectively suppress electrolyte leakage are preferred over liquid electrolytes. However, their ionic transport properties in the non-fluid state must be further optimized to maintain fast switching kinetics and long-term cycling stability. Finally, encapsulation strategies that provide long device lifetime and resistance to environmental factors such as humidity and temperature fluctuations are essential for reliable operation under real-world conditions.

Conclusion

In conclusion, WO_3 energy storage devices utilizing varying WiBS electrolyte compositions (10 M Zn + (0 to 7 M) Al) were successfully fabricated, and their electrical as well as EC properties were comprehensively investigated. The electrochemical and spectroscopic analyses confirmed the active participation of both Al^{3+} and Zn^{2+} ions during the coloration process, with the optimized 10 M Zn + 3 M Al electrolyte delivering superior performance. The device achieved a high energy storage capacity of 146 mAh/m^2, an optical contrast of 80.5%, a coloration efficiency of 35.3 cm^2/C, and stable cycling performance with 60% capacity retention after 800 cycles and 75% electrochromic stability. This study demonstrated that both Al^{3+} and Zn^{2+} ions contributed to the energy storage and EC performance of the devices, with Al^{3+} ions acting as a stabilizing booster at an optimal concentration to improve lattice stability and long-term durability. Beyond performance optimization, this work further highlighted the commercialization and interdisciplinary potential of WiBS-based WO_3 energy storage systems. The use of aqueous electrolytes and earth-abundant elements such as Zn and Al ensured material sustainability, safety, and cost-effectiveness, while the compatibility of WO_3 thin films with scalable coating techniques and large-area architectural glass supported practical integration. In addition, the excellent electrochemical stability of the WiBS electrolyte provides a solid foundation for next-generation devices, including energy storage smart

windows, adaptive display panels, and responsive energy storage systems capable of real-time energy level monitoring[14,57,58].

Data availability

All data generated or analyzed during this study are included in this published article.

Received: 30 July 2025; Accepted: 1 April 2026
Published online: 10 April 2026

References

1. Eldjilali, C. Z. et al. Electrochromic performances of TiO2 nanocrystals thin films for smart glass applications. *Thin Solid Films*. **815**, 140636. https://doi.org/10.1016/j.tsf.2025.140636 (Apr. 2025).
2. Tan, M. Y., Thien, G. S. H., Tan, K. B., Murthy, H. C. A. & Chan, K. Y. Investigation of electrochromic performances of multicolor V2O5 devices fabricated at low processing temperature. *Sci. Rep.* **15** (1), 1184. https://doi.org/10.1038/s41598-024-85014-7 (Jan. 2025).
3. Gu, C., Jia, A. B., Zhang, Y. M. & Zhang, S. X. A. Emerging Electrochromic Materials and Devices for Future Displays, (2022). https://doi.org/10.1021/acs.chemrev.1c01055
4. Yang, P., Sun, P. & Mai, W. Electrochromic energy storage devices. *Mater. Today*. **19** (7), 394–402. https://doi.org/10.1016/J.MATTOD.2015.11.007 (Sep. 2016).
5. Li, H., Firby, C. J. & Elezzabi, A. Y. Rechargeable Aqueous Hybrid Zn2+/Al3 + Electrochromic Batteries. *Joule* **3** (9). https://doi.org/10.1016/j.joule.2019.06.021 (2019).
6. Vulusala, V. S. & Madichetty, S. G and Application of superconducting magnetic energy storage in electrical power and energy systems: a review, (2018). https://doi.org/10.1002/er.3773
7. Nikolaos, P. C., Marios, F. & Dimitris, K. A Review of Pumped Hydro Storage Systems, (2023). https://doi.org/10.3390/en16114516
8. Liyakath Ali, N. U. H. et al. Porous boron-oxy-carbide hybrid nanosheets: a novel electrode material for high-performance wearable supercapacitors. *Adv. Compos. Hybrid. Mater.* **8** (3), 254. https://doi.org/10.1007/s42114-025-01337-7 (Jun. 2025).
9. Vignesh, K. et al. Oxygen-rich functionalized porous carbon by KMnO4 activation on pods of Prosopis juliflora for symmetric supercapacitors. *J. Energy Storage*. **72**, 108216. https://doi.org/10.1016/j.est.2023.108216 (Nov. 2023).
10. Mohanty, R., Parida, K. & Parida, K. Redox mediator-enhanced charge storage in dimensionally tailored nanostructures towards flexible hybrid solid-state supercapacitors. *Nanoscale Adv.* **5**, 4521–4535. https://doi.org/10.1039/D3NA00279A (2023).
11. Mohanty, R. & Parida, K. Carbamide-mediated facile sol-gel synthesis of porous flower-like ZnCo2O4 microspheres for high-performance asymmetric coin cell supercapacitors. *Electrochim. Acta*. **491**, 144327. https://doi.org/10.1016/j.electacta.2024.144327 (Jul. 2024).
12. Li, S. et al. Stable Zn–WO3 battery with a ZnCl2 water-in-salt electrolyte. *J. Power Sources*. **560** https://doi.org/10.1016/j.jpowsour.2023.232691 (2023).
13. Wang, Y., Meng, X., Sun, J., Liu, Y. & Hou, L. Recent Progress in 'Water-in-Salt' Electrolytes Toward Non-lithium Based Rechargeable Batteries, (2020). https://doi.org/10.3389/fchem.2020.00595
14. Wu, W. et al. Electrochromic devices constructed with water-in-salt electrolyte enabling energy-saving and prolonged optical memory effect. *Chem. Eng. J.* **446** https://doi.org/10.1016/j.cej.2022.137122 (2022).
15. Ejigu, A., Le Fevre, L. W. & Dryfe, R. A. W. Reversible Electrochemical Energy Storage Based on Zinc-Halide Chemistry. *ACS Appl. Mater. Interfaces*. **13** (12). https://doi.org/10.1021/acsami.0c20622 (2021).
16. Tong, Z. et al. A Ca-Ion Electrochromic Battery via a Water-in-Salt Electrolyte. *Adv. Funct. Mater.* **31** (41). https://doi.org/10.1002/adfm.202104639 (2021).
17. González, M. A. et al. Nanoscale Relaxation in 'water-in-Salt' and 'water-in-Bisalt' Electrolytes. *J. Phys. Chem. Lett.* **11** (17). https://doi.org/10.1021/acs.jpclett.0c01765 (2020).
18. Kartha, T. R., Reddy, D. N. & Mallik, B. S. Insights into the structure and ionic transport in 'water-in-bisalt' electrolytes for lithium-ion batteries. *Mater. Adv.* **2** (23). https://doi.org/10.1039/d1ma00572c (2021).
19. Forero-Saboya, J., Hosseini-Bab-Anari, E., Abdelhamid, M. E., Moth-Poulsen, K. & Johansson, P. Water-in-bisalt electrolyte with record salt concentration and widened electrochemical stability window. *J. Phys. Chem. Lett.* **10** (17). https://doi.org/10.1021/acs.jpclett.9b01467 (2019).
20. Suo, L. et al. Advanced High-Voltage Aqueous Lithium-Ion Battery Enabled by 'Water-in-Bisalt' Electrolyte, *Angewandte Chemie - International Edition*. 55(**25**) https://doi.org/10.1002/anie.201602397 (2016).
21. Xu, X. et al. Insight into the solvation and dynamic behaviors of lithium salt in water-in-bisalt electrolytes. *J. Mol. Liq.* **400** https://doi.org/10.1016/j.molliq.2024.124533 (2024).
22. Eric, H., Li, H. & Adulhakem, E. Rechargeable Zn2+/Al3 + dual-ion electrochromic device with long life time utilizing dimethyl sulfoxide (DMSO)-nanocluster modified hydrogel electrolytes. *RSC Adv.* **9** (55). https://doi.org/10.1039/c9ra06785j (2019).
23. Guo, J. et al. Prominent Electrochromism Achieved Using Aluminum Ion Insertion/Extraction in Amorphous WO3 Films. *J. Phys. Chem. C.* **122** (33). https://doi.org/10.1021/acs.jpcc.8b05692 (2018).
24. Thongpan, W. et al. Porous CuWO4/WO3 composite films with improved electrochromic properties prepared by sparking method. *Mater. Lett.* **257** https://doi.org/10.1016/j.matlet.2019.126747 (2019).
25. Wen-Cheun Au, B., Tamang, A., Knipp, D. & Chan, K. Y. Post-annealing effect on the electrochromic properties of WO3 films. *Opt. Mater. (Amst).* **108** https://doi.org/10.1016/j.optmat.2020.110426 (2020).
26. Xie, Z., Zhang, Q., Liu, Q., Zhai, J. & Diao, X. Enhanced electrochromic performance of 2D grid-structured WO3 thin films. *Thin Solid Films*. **653** https://doi.org/10.1016/j.tsf.2018.03.044 (2018).
27. Purushothaman, K. K., Muralidharan, G. & Vijayakumar, S. Sol-Gel coated WO3 thin films based complementary electrochromic smart windows. *Mater. Lett.* **296** https://doi.org/10.1016/j.matlet.2021.129881 (2021).
28. Au, B. W. C., Chan, K. Y. & Pang, W. L. Electrochromic properties of WO3 films based on lithium iodide and lithium perchlorate polymer electrolyte. *Optik (Stuttg).* **225** https://doi.org/10.1016/j.ijleo.2020.165769 (2021).
29. Abdelhamed, A. H. E. et al. Jan., Solution Casting Effect of PMMA-Based Polymer Electrolyte on the Performances of Solid-State Electrochromic Devices, *Polymers (Basel).* 17(1) p. 99. https://doi.org/10.3390/polym17010099 (2025).
30. Zhang, W., Li, H., Yu, W. W. & Elezzabi, A. Y. Transparent inorganic multicolour displays enabled by zinc-based electrochromic devices. *Light Sci. Appl.* **9** (1). https://doi.org/10.1038/s41377-020-00366-9 (2020).
31. Yao, H. R., You, Y., Yin, Y. X., Wan, L. J. & Guo, Y. G. Rechargeable dual-metal-ion batteries for advanced energy storage, (2016). https://doi.org/10.1039/c6cp00586a
32. Qu, H. et al. One-pot preparation of crystalline-amorphous double-layer structured WO3 films and their electrochromic properties. *Electrochim. Acta*. **148** https://doi.org/10.1016/j.electacta.2014.10.017 (2014).
33. Wen-Cheun Au, B., Chan, K. Y. & Knipp, D. Effect of film thickness on electrochromic performance of sol-gel deposited tungsten oxide (WO3). *Opt. Mater. (Amst).* **94** https://doi.org/10.1016/j.optmat.2019.05.051 (2019).

34. Kubovics, M. et al. Role of Graphene Oxide Aerogel Support on the CuZnO Catalytic Activity: Enhancing Methanol Selectivity in the Hydrogenation Reaction of CO2. *ChemCatChem* **14** (18). https://doi.org/10.1002/cctc.202200607 (2022).
35. Zhang, Q. et al. One-Pot' Construction of Networked AlCl3·6H2O@β-CD Composites by Mechanical Milling: A Green and Efficient Catalyst for the Synthesis of Bisindolylmethane Compounds. *Catal. Lett.* **154** (1). https://doi.org/10.1007/s10562-023-04297-z (2024).
36. Chen, P., Baldwin, M. & Bandaru, P. R. Hierarchically structured, oxygen deficient, tungsten oxide morphologies for enhanced photoelectrochemical charge transfer and stability. *J. Mater. Chem. Mater.* **5** (28). https://doi.org/10.1039/c7ta04118g (2017).
37. Gupta, S. P. et al. Morphology and crystal structure dependent pseudocapacitor performance of hydrated WO3nanostructures. *Mater. Adv.* **1** (7). https://doi.org/10.1039/d0ma00518e (2020).
38. Nguyen, T. H. Q. et al. Enhancing the Spectroelectrochemical Performance of WO3 Films by Use of Structure-Directing Agents during Film Growth. *Appl. Sci. (Switzerland)*. **12** (5). https://doi.org/10.3390/app12052327 (2022).
39. Aldrees, A., Khan, H., Alzahrani, A. & Dan'azumi, S. Synthesis and characterization of tungsten trioxide (WO3) as photocatalyst against wastewater pollutants. *Appl. Water Sci.* **13** (7). https://doi.org/10.1007/s13201-023-01938-x (2023).
40. Bao, X. et al. A deep eutectic electrolyte of AlCl3-acetamide for rechargeable aluminum-ion batteries. *New J. Chem.* https://doi.org/10.1039/d4nj00147h (2024).
41. Li, W. et al. Dec., Electrochemical Failure Results Inevitable Capacity Degradation in Li-Ion Batteries—A Review, *Energies (Basel).* 15(23) p. 9165. https://doi.org/10.3390/en15239165 (2022).
42. Zhou, X., Ma, K., Zhang, Q., Yang, G. & Wang, C. Highly stable aqueous zinc-ion batteries enabled by suppressing the dendrite and by-product formation in multifunctional Al3 + electrolyte additive, *Nano Res. 15(9)* pp. 8039–8047. https://doi.org/10.1007/s12274-022-4419-y Sep. (2022).
43. Del Olmo, D., Pavelka, M. & Kosek, J. Open-Circuit Voltage Comes from Non-Equilibrium Thermodynamics. *J. Non-Equilib. Thermodyn.* **46** (1). https://doi.org/10.1515/jnet-2020-0070 (2021).
44. Chen, Y., Chen, K. Y. & Tseung, A. C. C. Electrochemical alcohol sensor based on a co-electrodeposited Pt|WO3 electrode. *J. Electroanal. Chem.* **471** (2). https://doi.org/10.1016/S0022-0728(99)00271-5 (1999).
45. Wang, B. et al. A Long-Life Battery-Type Electrochromic Window with Remarkable Energy Storage Ability. *Solar RRL*. **4** (3). https://doi.org/10.1002/solr.201900425 (2020).
46. Wang, L. et al. A new design of an electrochromic energy storage device with high capacity, long cycle lifetime and multicolor display. *J. Mater. Chem. Mater.* **8** (33). https://doi.org/10.1039/d0ta04824k (2020).
47. Liu, Y. et al. Rechargeable aqueous Zn-based energy storage devices, (2021). https://doi.org/10.1016/j.joule.2021.10.011
48. Nanjo, C., Yokogawa, D., Matsushita, M. M. & Awaga, K. Chemical potentials of electric double layers at metal-electrolyte interfaces: dependence on electrolyte concentration and electrode materials, and application to field-effect transistors. *Phys. Chem. Chem. Phys.* **22** (22). https://doi.org/10.1039/d0cp00423e (2020).
49. Casebolt, R. et al. Effect of Electrolyte Composition and Concentration on Pulsed Potential Electrochemical CO2 Reduction. *ChemElectroChem* **8** (4). https://doi.org/10.1002/celc.202001445 (2021).
50. Ahn, H., Kim, D., Lee, M. & Nam, K. W. Challenges and possibilities for aqueous battery systems, (2023). https://doi.org/10.1038/s43246-023-00367-2
51. Zhang, C. et al. A ZnCl2 water-in-salt electrolyte for a reversible Zn metal anode. *Chem. Commun.* **54** (100). https://doi.org/10.1039/c8cc07730d (2018).
52. Jiao, Z. et al. Electrochromic properties of nanostructured tungsten trioxide (hydrate) films and their applications in a complementary electrochromic device. *Electrochim. Acta*. **63** https://doi.org/10.1016/j.electacta.2011.12.069 (2012).
53. Tan, M. Y. et al. Rapid post-annealing effect on the TiO2-based electrochromic films. *Opt. Mater. (Amst)*. **145** https://doi.org/10.1016/j.optmat.2023.114455 (2023).
54. More, A. J. et al. Electrodeposition of nano-granular tungsten oxide thin films for smart window application. *Mater. Lett.* **134** https://doi.org/10.1016/j.matlet.2014.07.059 (2014).
55. Cai, G., Darmawan, P., Cheng, X. & Lee, P. S. Inkjet Printed Large Area Multifunctional Smart Windows. *Adv. Energy Mater.* **7** (14). https://doi.org/10.1002/aenm.201602598 (2017).
56. Ganesha, M. K., Mondal, I., Singh, A. K. & Kulkarni, G. U. Fabrication of Large-Area, Affordable Dual-Function Electrochromic Smart Windows by Using a Hybrid Electrode Coated with an Oxygen-Deficient Tungsten Oxide Ultrathin Porous Film, *ACS Appl. Mater. Interfaces.* 15(**15**) pp 19111–19120. https://doi.org/10.1021/acsami.2c22638 Apr. (2023).
57. Gong, H., Wang, S., Xie, M. & Wang, H. An aqueous aluminum-ion electrochromic energy storage device with visual energy level. *Sol. Energy Mater. Sol. Cells*. **248** https://doi.org/10.1016/j.solmat.2022.112018 (2022).
58. Song, Z. et al. Fast and Stable Zinc Anode-Based Electrochromic Displays Enabled by Bimetallically Doped Vanadate and Aqueous Zn2+/Na+ Hybrid Electrolytes. *Nanomicro Lett.* **15** (1), 229. https://doi.org/10.1007/s40820-023-01209-z (Dec. 2023).

Author contributions

Ming-Yue Tan (Conceptualization, Experimental, Data Curation, Investigation, Data Analysis, Original manuscript writing, Manuscript Revision and Review), Gregory Soon How Thien (Experimental, Dat Curation, Visualization), Kar Ban Tan (Characterization System Support, Manuscript Revision and Review, Validation), Ab Rahman Marlinda (Characterization System Support, Manuscript Revision and Review, Validation), Mohd Sufri Mastuli (Characterization System Support, Manuscript Revision and Review, Validation), H.C. Ananda Murthy (Manuscript Revision and Review, Visualization, Validation), B S Surendra (Manuscript Revision and Review, Visualization, Validation), Yun Ii Go (Manuscript Revision and Review, Visualization, Validation), Kah-Yoong Chan (Conceptualization, Investigation, Data Analysis, Manuscript Revision and Review, Visualization, Validation, Funding, Project Management, Supervision).

Funding

This work was funded by the Telekom Malaysia Research and Development (TM R&D) under TM R&D Research Fund (Grant No: RDTC/261168, Project ID: MMUE/260004).

Declarations

Competing interests

The authors declare no competing interests.

Additional information

Supplementary Information The online version contains supplementary material available at https://doi.org/1

0.1038/s41598-026-47561-z.

Correspondence and requests for materials should be addressed to K.-Y.C.